Connectivity-consistent mapping method for 2-D discrete fracture networks

Delphine Roubinet, Jean-Raynald de Dreuzy, Philippe Davy

Connectivity-consistent mapping method for 2D discrete fracture networks

Delphine Roubinet, Jean-Raynald de Dreuzy and Philippe Davy

Geosciences Rennes, UMR CNRS 6118, Université de Rennes I, Rennes, France

Abstract

We present a new flow computation method in 2D Discrete Fracture Networks (DFN) intermediary between the classical DFN flow simulation method and the projection onto continuous grids. The method divides the simulation complexity by solving for flows successively at a local mesh scale and at the global domain scale. At the mesh scale, flows are determined by classical DFN flow simulations and approximated by an Equivalent Hydraulic Matrix (EHM) relating heads and flow rates discretized on the mesh borders. Assembling the Equivalent Hydraulic Matrices provides for a domain-scale discretization of the flow equation. The Equivalent Hydraulic Matrices transfer the connectivity and flow structure complexities from the mesh scale to the domain scale. Compared to existing geometrical mapping or equivalent tensor methods, the EHM method broadens the simulation range of flow to all types of 2D fracture networks both below and above the Representative Elementary Volume (REV). Additional computation linked to the derivation of the mesh-scale Equivalent Hydraulic Matrices increases the accuracy and reliability of the method. Compared to DFN methods, the EHM method first provides a simpler domain-scale alternative permeability model. Second, it enhances the simulation capacities to larger fracture networks where flow discretization on the DFN structure yields system sizes too large to be solved using the most advanced multigrid and multifrontal methods. We show that the EHM method continuously moves from the DFN method to the tensor representation as a function of the mesh-scale discretization. The balance between accuracy and model simplification can be optimally controlled by adjusting the domain-scale and mesh-scale discretizations.

1. Introduction

Fractured media has been classically modeled using either Discrete Fracture Network (DFN) or Stochastic Continuum (SC) approaches [*Neuman*, 2005]. Both approaches have their own advantages and drawbacks [*Hsieh*, 1998]. First, they differ by their underlying permeability structure and their capacity of being specified by existing field data [*Hsieh*, 1998]. The DFN approach easily accounts for extensive fracture characterization [*Cvetkovic et al.*, 2004; *Davy et al.*, 2006] while the SC approach copes more consistently with hydraulic data [*Ando et al.*, 2003]. Second, the simulation of hydraulic processes requires the development of specific methods using the DFN approach whereas only standard discretization schemes are required with the SC approach. Third, because the SC approach simplifies the fracture network structure, it is generally less computationally demanding than the DFN method. Hybrid approaches have been developed to combine the advantages of the DFN and SC approaches. Most of them use a DFN approach at the onset for building equivalent heterogeneous continuous models mapping either the smallest fractures [*Lee et al.*, 2001] or all fractures in the case of the Fracture Continuum Model (FCM) [*Botros et al.*, 2008; *Bourbiaux et al.*, 1998; *Jackson et al.*, 2002; *Reeves et al.*, 2008; *Svensson*, 2001]. Fracture Continuum Models aim at benefiting both from the structure complexity of DFNs and from the simulation and computational simplicities of continuous media. The objective is often to use the FCM approximation as a basis for simulating more computationally demanding transient or multiphase flows [*Bourbiaux et al.*, 1998; *Karimi-Fard et al.*, 2006].

The quality of the FCM models critically depends on the derivation of the block-scale permeabilities from the DFNs, i.e. on the mapping of the fracture network onto the continuum grid. The block is considered here as the elementary cell of the continuum grid. Block-scale permeabilities are obtained either from geometrical characteristics [*Botros et al.*, 2008; *Svensson*, 2001] or through block-scale

48 numerical simulations of flow [*Jackson et al.*, 2002]. Potential errors stem from differences between
49 the derived scalar or tensor permeabilities and the effective flows within the block. They arise from
50 the difficulty to account for complex fracture connectivity on a broad range of scales. For mapping
51 based on geometrical rules, errors decrease with finer discretization whereas for mapping based on
52 hydraulic computation of the equivalent permeability tensor, errors increase below the
53 Representative Elementary Volume [*Long et al.*, 1982]. *Jackson et al.* [2002] corrected part of the
54 latter error by using a larger simulation zone, namely the "guard zone", designed to remove dummy
55 additional fracture connectivity with the sides of the block. FCMs keep the general connectivity
56 structure above the scale of the block but remove most of the connectivity effects at lower scales.
57 This results in less flow localization at the block scale and in difficulties in defining an equivalent
58 block permeability tensor. A simple assessment criterion of the relevance of the tensor representation
59 is the difference between flows on opposite block faces. They are equal in the tensor representation.
60 Their difference is expected to increase steeply for complex networks below the REV scale as shown
61 in the example of Figure 1. To avoid handling complex connectivity at the block scale, existing FCM
62 methods are applied either at scales close to the smallest fractures modeled [*Botros et al.*, 2008;
63 *Reeves et al.*, 2008] or at scales larger than the Representative Elementary Volume (REV)
64 [*Durlofsky*, 1991; *Jackson et al.*, 2002]. The first methods, i.e. the methods applicable to scales close
65 to the smallest fracture modeled, represent permeability by a scalar or a diagonal tensor. They
66 require fine grids for fractured medium representation but can be highly accurate for not too dense
67 fracture networks [*Botros et al.*, 2008]. The second methods, i.e. the methods applicable to scales
68 larger than the REV, represent permeability by an anisotropic full tensor defined by three 2D
69 parameters K_{xx}, K_{yy} and $K_{xy}=K_{yx}$. They require the a priori knowledge of the REV and are hence more
70 suited to dense fracture networks. Their drawbacks are the strong homogenization of flow, their
71 applicability to a restricted scale range and the increase of the numerical error with the refinement of
72 discretization.

None of these methods applies between the scale of the smallest fractures modeled and the REV, a scale range that spans orders of magnitude for multiscale fracture networks (i.e. fracture networks for which the fracture-length distribution is a power law) [*Bonnet et al.*, 2001; *de Dreuzy et al.*, 2001b]. In fact, this scale range extends at least from the connectivity scale to the REV scale. The connectivity scale is the scale at which networks are just connected. It ranges from meters to kilometers [*Berkowitz et al.*, 2000; *Davy et al.*, 2009]. Because of the fracture transmissivity variability, the REV scale can be one to three orders of magnitude larger than the connectivity scale [*Baghbanan and Jing*, 2007; *de Dreuzy et al.*, 2001a; 2002]. Extending at least from the scales contributing to connectivity to the REV scale, the scale range of fractures contributing to flow covers several orders of magnitude from the meter to the kilometer scale. For this scale range, the only available flow simulation method is the DFN method. The DFN flow simulation method, however, is limited in terms of fracture number and domain size. The limiting step arises when solving the linear system issued from the flow discretization on the network structure. With traditional system-solving methods like the conjugate gradient, limitations stemmed from computation time. However, the new numerical methods like the multifrontal or algebraic multigrid method, as implemented in UMFPACK [*Davis*, 2004] and HYPRE [*Falgout et al.*, 2005], are orders of magnitude faster but require additional memory [*de Dreuzy and Erhel*, 2002]. Their sole limitation is the computer memory. As a rule of thumb, they can solve at most a linear system of rank one million in a couple of minutes on a personal workstation (Pentium Xeon, 3 GHz, 8 Go). Consequently, improving simulation capacities is not about speeding up the method but about enabling simulations otherwise impossible because of memory requirements. We will thus look in this paper at the numerical memory complexity rather than at the numerical time complexity. Our longer-term strategy is to use parallel computing for performing Monte-Carlo simulations while sequential individual simulations remain sequential [*Erhel et al.*, 2009]. This ensures scalability and a minimum of parallel computing implementation.

We propose a new FCM method for the scale range where no existing FCM method is applicable. Like with the previously-cited FCM methods, the objective is to simplify the domain-scale numerical scheme and computations while keeping the complexity of the DFN structure. The new method divides the simulation complexity by solving for flows successively at the local block scale and at the global domain scale. At the block scale, flows are determined by classical DFN flow simulations and approximated by an Equivalent Hydraulic Matrix (EHM) relating heads and flow rates discretized on the mesh borders. Assembling the Equivalent Hydraulic Matrices allows for a domain-scale discretization of the flow equation. The Equivalent Hydraulic Matrices transfer the connectivity and flow structure complexities from the block scale to the domain scale. The method is similar to Boundary Element Methods [*Dershowitz and Fidelibus*, 1999] as it relates heads and flow rates on the block borders. As the Equivalent Hydraulic Matrices are determined at the block scale by DFN simulations, we show that the method is systematically applicable regardless of the scale, fracture density and fracture-length and transmissivity distributions. The method accuracy and complexity are given by the level of discretization of the block borders and of the domain. We call this method the Equivalent Hydraulic Matrices (EHM) method as heads and flow rates on the block borders are linearly linked by a matrix representing the block-scale hydraulic properties rather than by a scalar or a tensor permeability. This article describes the EHM method (section 2), shows its results compared to existing methods (section 3) and discusses its performance (section 4).

2. The Equivalent Hydraulic Matrices method

This section defines the EHM method. Once the domain meshed into elementary blocks, the principle of the EHM method is to express the block-scale hydraulic properties by a linear relationship between discretized flow rates and heads on the block borders. This expression will replace the scalar or tensor models used in classical FCM models. With $\boldsymbol{p_k}$ as the discretization points (also called poles) of the block numbered *k*, the vector of flow rates $\boldsymbol{\phi_k}$ and heads $\boldsymbol{H_k}$ on these

122 points are related by the following linear relationship:

123 $$\boldsymbol{\phi_k} = \boldsymbol{A_k} \cdot \boldsymbol{H_k}. \quad (1)$$

124 The block matrix $\boldsymbol{A_k}$ contains sub-block scale connectivity information and can be considered as the
125 block-scale constitutive relationship. It is obtained by performing block-scale flow simulations on
126 the DFN. Once obtained, the block-scale matrices $\boldsymbol{A_k}$ are used for simulating flow rates at the system
127 scale by imposing the continuity of heads and flow rates across the block borders. Relationship (1)
128 differs a priori from Darcy's law by its relating flow rates to heads and not to head gradients. This is
129 only a surface difference since the construction method (section 2.2) and the resulting properties of
130 matrices $\boldsymbol{A_k}$ (Appendix A) ensure a dependence of the flow rates on head gradients.

131 **2.1. Discretization**

132 Discretization is made up of two parts consisting in discretization of the domain into elementary
133 blocks (classical meshes) and discretization of block borders into poles. The first discretization
134 consists in defining the mesh of the Fracture Continuum Model. We use hereafter a regular grid even
135 though the EHM method can cope with irregular meshes. Each mesh cell will be called a block. The
136 block contains a subset of the fracture network, i.e. a sub-network, the intersections of which with
137 the block limits are denoted $\boldsymbol{m_k}$. $\boldsymbol{m_k}(i)$ is the i^{th} intersection of block k. The second discretization
138 consists in splitting up the block borders into segments of constant length d_{block}, the discretization of
139 each border starting at the border corner. Each segment contains either zero, one or more than one
140 fracture border intersection $\boldsymbol{m_k}(i)$. We define poles $\boldsymbol{p_k}$ as the centers of those segments containing at
141 least one intersection (Figure 2). Segments containing no intersection with the subnetwork are
142 disregarded. The fundamental principle of the EHM method is that all intersections contained in the
143 same segment are set to the same hydraulic head corresponding to the head of the pole. These
144 additional equalities reduce the number of unknowns at the cost of the approximation that close

intersections have the same hydraulic head. The accuracy of the approximation is function of the block discretization ratio r_{block} defined as the block-border discretization scale d_{block} normalized by the block face length. The coarsest discretization corresponds to r_{block}=100% and gives a single pole by block face. It leads to a representation close to the tensor representation (Figure 2a). It is, however, not equal to a tensor. First, opposite fluxes may not be equal. Second, some faces may not be intersected by the network and thus may not have led to a pole. Finer discretizations, obtained for decreasing r_{block} values, lead to more accurate representations converging to the DFN method when all poles correspond exactly to one intersetion (Figure 2b). Like in classical numerical methods, we will show in section 3 that the numerical error of the EHM method decreases monotonously with the block-border discretization ratio r_{block}, i.e. when shifting from tensor-like to DFN methods.

2.2. Construction of the block-scale Equivalent Hydraulic Matrices

Equivalent Hydraulic Matrix $\boldsymbol{A_k}$ expresses the linear relationship between flows and heads on the block border discretization. More specifically, by developing relationship (1), coefficient $\boldsymbol{A_k}(i,j)$ is the contribution of the head at the j^{th} pole to the flow at the i^{th} pole:

$$\boldsymbol{\phi_k}(i) = \sum_{j=1}^{N_P^k} \boldsymbol{A_k}(i,j) \cdot \boldsymbol{H_k}(j). \qquad (2)$$

where N_P^k is the pole number of block k and $\boldsymbol{\phi_k}(i)$ and $\boldsymbol{H_k}(i)$ are the flow rate and head, respectively, at i^{th} pole $\boldsymbol{p_k}(i)$. $\boldsymbol{A_k}(i,j)$ is also equal to the flow rate computed at pole i by imposing a fixed head of 1 at pole j and 0 at the other ones, i.e. a fixed head of 1 for the intersections overlapped by the segment centered on pole j and 0 for the other ones. With these boundary conditions, all coefficients of column j can be simultaneously determined by a single DFN simulation (Figure 3). The construction of the full Equivalent Hydraulic Matrix requires $N_P^k - 1$ simulations and not N_P^k, since the sum of all elements from a column of $\boldsymbol{A_k}$ is equal to zero because of flow conservation

(Appendix A). We underline that this method does not require any modification of the fracture network structure or any realignment of fractures. The approximation lies exclusively in equating flows and heads at the scale of the segment of the border discretization.

2.3. Domain-scale flow simulation

Solving the flow equation at the domain scale consists in imposing the continuity of heads and flow rates on poles $\boldsymbol{p_k}$ positioned on the block faces. External head and flow rate boundary conditions are simply implemented by imposing the head in the matrix system for the fixed head values and by adding a source term for the fixed flow rates on the corresponding poles, respectively.

We note P the union of all pole points $\boldsymbol{p_k}$ with the convention that poles common to two or more blocks occur only once in P. P is made up of N^{i} poles at the interface between two blocks (P^{i}) and of N^{f} poles at the physical limits of the domain (P^{f}). The total number of poles at the domain scale N is equal to the sum of poles of types P^i and P^f:

$$N = N^i + N^f. \tag{3}$$

With $B(j)$ as the set of blocks sharing pole $P^i(j)$ and with $q_{b,P^i(j)}$ as the flow rate at pole $P^i(j)$ from the b^{th} block of $B(j)$, flow continuity writes:

$$\sum_{b\,\epsilon\,B(j)} q_{b,P^i(j)} = 0\ \forall j \epsilon\ [\![1, N^i]\!]. \tag{4}$$

For the N^{fd} fixed poles at the domain limit where a Dirichlet boundary condition is applied:

$$H^{fd} = (H^{fd})_0. \tag{5}$$

For the N^{fn} poles on the Neumann boundary condition, the imposed flow is simply inserted in

186 equation (4). Equations (1), (4) and (5) lead to a linear system of N equations of the N unknown
187 heads at the poles.

188 The first advantage of the EHM method compared to existing Fracture Continuum Models (FCMs)
189 is the conservation of connectivity between blocks. In fact, faces intersected by fractures contain at
190 least one pole whereas faces without intersecting fractures do not have any pole. This prevents
191 dummy additional connectivity between blocks [*Jackson et al.*, 2002; *Reeves et al.*, 2008]. The
192 second advantage of the EHM method is the existence of block-scale discretization parameter r_{block},
193 which can be used to tune the balance between numerical efficiency and accuracy. The third
194 advantage of the method is the systematic convergence with discretization and its adjustment to all
195 kinds of 2D synthetic fracture networks as will be shown in section 3. The main drawbacks of the
196 EHM method are the necessity to perform block-scale DFN flow simulations and the specificity of
197 the domain-scale flow simulation that precludes the use of standard softwares like MODFLOW.

198 **3. Results**

199 **3.1. Fracture network types**

200 The tested networks have been chosen so that they cover a wide range of networks both above and
201 below the REV scale, with broad and narrow length and transmissivity distributions (Table 1).
202 Extreme cases of low and high variability are tested in order to assess the method in highly-
203 differentiated conditions. Network types include both lattice structures (Table 2.I1) and stochastic
204 complex fracture networks (Table 2.I2-4). Stochastic fracture networks are characterized by their
205 density, orientation, length and transmissivity distributions. The domain size given by the ratio of the
206 domain length to the minimal fracture length is denoted by L and set to 100. It means that the
207 fracture length distribution covers two orders of magnitude. Density is fixed by the dimensionless
208 percolation parameter p, equal to the sum of the square of the fracture lengths normalized by the

domain area. p is a direct measure of connectivity as it is very close to 5.6 at the percolation threshold, whatever the other fracture network characteristics [*Bour and Davy*, 1997]. Three density values are used for stochastic complex fracture networks and are respectively close to threshold (p=6) and at around two and three times the density at threshold (p=10 and p=20). For lattice structures, p is close to the number of fractures within the domain and has been chosen equal to 12 and 192 for testing methods on sparse and dense lattices, respectively. Orientations are set to 0° and 30° relative to the main flow directions for the lattice structures and are uniformly distributed for the complex stochastic fracture networks. For the complex stochastic fracture networks, fracture lengths are power-law distributed [*Bonnet et al.*, 2001] according to the following distribution function:

$$p(l) \sim l^{-a} \tag{6}$$

where l is the fracture length, a is the characteristic power-law length exponent and $p(l)$ the fracture number of length l. Natural values of a derived from outcrops range in the interval [2.0,3.5]. Fracture transmissivity values have been chosen to be either the same for all fractures or broadly distributed according to a lognormal distribution of logarithmic standard deviation equal to 3 [*Tsang et al.*, 1996]. Flow boundary conditions are classical gradient-like boundary conditions with fixed head on two opposite domain faces and a constant head gradient on the orthogonal faces (Figure 1a). The bottom line of Table 2 illustrates the flow distribution computed with a broad transmissivity distribution and shows the strong channeling induced by the transmissivity distribution.

3.2. Comparison criteria

For comparing the performance of the EHM method with other existing methods, we use an accuracy criterion and a numerical memory complexity criterion. Accuracy is defined as the mean difference between the inlet and outlet flows and their reference counterparts. The reference is obtained from

231 the direct simulation on the domain-scale discrete fracture network. By denoting $\Phi_m^{f_i}$ and $\Phi_{ref}^{f_i}$ the
232 flow rates obtained respectively by the method "*m*" and the reference method on face f_i, the
233 comparison criterion writes:

234 $$flow\_error_m = \frac{1}{2}\left(\left|\frac{\Phi_m^{f_l}-\Phi_{ref}^{f_l}}{\Phi_{ref}^{f_l}}\right| + \left|\frac{\Phi_m^{f_r}-\Phi_{ref}^{f_r}}{\Phi_{ref}^{f_r}}\right|\right) \times 100 \quad (7)$$

235 where f_l and f_r stand for the left and right vertical domain faces.

236 The memory complexity criterion is taken as the number of non-zero elements *nnz* of matrix *B* in the
237 linear system *Bx=b* issued from the discretization of the flow equation at the domain scale. Even if
238 the number of non-zero elements is not the ideal criterion, it is still better than the system size in this
239 case where the limitation lies rather in memory requirements than in computation time. All results
240 represent averages over 10 simulations. We have checked that for the most complex cases *D0* and
241 *D1*, 10 and 100 simulations give very close results. Accuracy and numerical memory complexity
242 results are computed for several discretizations characterized by the number of blocks (domain-scale
243 discretization) and by r_{block} (block-scale discretization).

244 **3.3. Results with existing mapping and tensor methods**

245 To assess the Equivalent Hydraulic Matrices method, we compare it with other existing methods:
246 first with what we call the ANIS_GEO method representing permeability by a diagonal tensor
247 derived from fracture geometrical mapping onto the blocks and used within a finite volume method
248 [*Botros et al.*, 2008] and second with what we call the TENSOR_SIM method representing
249 permeability by a full tensor obtained from block-scale DFN flow simulations and used within a
250 mixed hybrid finite element framework (Appendix B). For these two methods, the matrix
251 permeability is fixed to 10^{-12} m/s. We use these two methods only when they are strictly applicable.

From [*Botros et al.*, 2008], the ANIS_GEO method is applicable only if the ratio of the block length to the minimal fracture length is lower than 2.5. For the stochastic complex networks (Table 1 B0-D1), the ratio of the domain size to the minimal fracture length is $L=100$, requiring for the ANIS_GEO method a domain-scale discretization of at least 40×40 blocks. As the TENSOR_SIM method relies on the full permeability tensor at the block scale, we have determined this parameter for all studied networks from the block-scale directional permeability plots (Table 3). The method is applicable only when the directional permeability is close to an ellipse [*Long et al.*, 1982]. It is the case for networks *A0*, *A2* and *D0* (Table 3). For the other networks, transmissivity and fracture length distributions display heterogeneities that cannot be represented by a tensor at the scale of the block.

Table 4 shows the flow error as measured by (7) using the ANIS_GEO, TENSOR_SIM and EHM methods for several domain discretizations. With the ANIS_GEO method, the flow error decreases systematically from a 50×50 to a 200×200 domain discretization. ANIS_GEO is particularly accurate for sparse flow structures (networks with a small fracture density or with a broad transmissivity distribution). In fact, the simple summation of the fracture contributions induced by the mapping increases sub-block-scale connectivity and hence increases flow errors. Results also show that ANIS_GEO is not applicable to networks with connectivity driven by small fractures ($3<a<3.5$), yielding errors systematically larger than 41%. To be applied systematically, the geometrical projection method ANIS_GEO requires high levels of discretization involving large linear systems (Table 5). Such discretization levels can be achieved in 2D but likely not in 3D.

The TENSOR_SIM method is accurate for regular and dense structures with an error lower than 1% for network *A0* (Table 4). As opposed to the ANIS_GEO method, the error decreases when the block scale increases since the block becomes closer and eventually larger than the REV [*Li et al.*, 2009]. The main drawback of this method is its highly limited range of application. Most of the tested

networks of Table 1 did not fulfill its conditions of application.

3.4. Assessment of the EHM method

We have tested two levels of block-scale discretization of the EHM method: $r_{block}=10\%$ (called the most accurate method) and $r_{block}=25\%$ (called the least accurate method). The EHM method gives much smaller errors than those given by the geometrical and tensor methods ANIS_GEO and TENSOR_SIM (Table 4) except for *A0* (dense lattice structure with uniform fracture transmissivity) and *D0* (dense fracture network with uniform fracture transmissivity) with a domain discretized by 10×10 blocks and r_{block}=25%. For these two cases, the tensor method gives smaller errors than the least accurate EHM method. In fact, the tensor method is very accurate because the REV is smaller than the block. The large errors of the least accurate EHM method are linked to the large number of fracture intersection points with the block border set to the same head, i.e. the head of the corresponding pole. The merged points are quantified by the border merging percentage p_{border} equal to the difference in percentage between the intersection point and pole numbers. p_{border} is 0% in the absence of any approximation of the block-scale discretization and increases as larger approximations are induced by the use of a smaller number of poles for the block-scale discretization. For *A0* and *D0* with the 10×10 domain discretization and r_{block}=25%, p_{border} is larger than 90% and 70%, respectively (Table 6). This explains the cases where the EHM method is less accurate than the TENSOR_SIM method. For the same networks with finer domain discretizations (30×30 and 50×50 blocks), trends are reversed and the EHM method becomes more accurate than the tensor method. For lattice cases, the flow error with the EHM method is smaller than 5% for a domain discretization of 50×50 blocks.

For stochastic complex fracture networks, flow errors range from 0.11% to 180% with a majority of errors below 10% (Table 4). Errors larger than 10% affect cases *B2* and *C2* characterized by a coarse

299 discretization of 10×10 blocks and by networks with the narrowest length distribution corresponding
300 to a=3.5. The latter fracture networks have the largest number of fractures and fracture border
301 intersections inducing first a stronger decrease in the numerical memory complexity (Table 5), and
302 then larger values of point merging percentages p_{border} (Table 6). In all other cases, the flow error is
303 smaller than 5% for a domain discretization of 50×50 blocks. With the most accurate method
304 corresponding to r_{block}=10% and a domain discretization of 50×50 blocks, errors range between
305 0.11% and 2.1%. For 9 out of the 12 test cases for which $\sigma_{lnT} = 3$ corresponds to a fracture
306 transmissivity distribution spanning at least 3 orders of magnitude, errors remain as low as a few
307 percents showing the very good performance of the EHM method for complex flow structures.

308 Results of Table 4 show two interesting properties of the EHM method. First, errors are not sensitive
309 to the fracture transmissivity distribution as shown by the comparison of the *D0* and *D1* cases.
310 Second, errors systematically decrease both with the domain discretization at constant r_{block} and with
311 r_{block} at constant domain discretization for all complex stochastic fracture networks. These properties
312 offer possibilities to control the error by decreasing either the domain-scale discretization in blocks
313 or the block-scale discretization ratio r_{block}. We note that all the above simulations have been
314 performed on the backbone. However the applicability of the EHM method is not restricted to the
315 backbone as shown by its good performance on infinite clusters (Table 7). Even if errors increase by
316 a factor of 5 from the backbone to the infinite cluster, they still remain lower than 10% with the least
317 accurate method (r_{block}*=10%*) and a domain discretization of 50×50.

318 **3.5. Flow error versus numerical memory complexity**

319 Numerical memory complexity is taken as the number of non-zero elements in the domain-scale
320 linear system issued from the discretization of the flow equation (*nnz*) (Table 5). *nnz* determines the
321 memory required to solve the linear system. It does not, however, take into account the computation

of the Equivalent Hydraulic Matrices at the block scale as they are not critical in terms of system size and memory requirements. With the classical ANIS_GEO and TENSOR_SIM methods, the numerical memory complexity increases quadratically with the discretization ratio. With the EHM method, the numerical memory complexity is more variable and increases more slowly. Whatever the domain discretization and the value of r_{block} for complex stochastic fracture networks, EHM methods yield smaller numerical memory complexity than the DFN method except for the *B0* case. In the latter case, the proportion of blocks crossed by a single fracture increases the numerical memory complexity without improving the accuracy.

A more advanced evaluation of the methods is proposed by comparing their error according to their numerical memory complexity (Figures 4-6). For lattice structures (Figure 4 except magenta symbols), the EHM method is orders of magnitude more accurate than the classical methods at comparable complexities except for the *A0* case already discussed in section 3.4. Figure 4 also shows that the accuracy of the TENSOR_SIM method increases with the numerical memory complexity as discussed in section 3.3. For the dense complex stochastic fracture network of case *D0* (Figure 4, magenta symbols), the error with the TENSOR_SIM method is smaller than the error with all other methods at very low complexity (11%) but cannot be made smaller by refining the discretization. By contrast, with the EHM method, the error is larger at small complexity but decreases to less than 1% for the highest complexities. For the stochastic complex fracture networks (Figures 5-6), errors with the EHM method decrease with the numerical memory complexity (*nnz*), with a systematic trend close to nnz^{-1}. Figures 4-6 show that the errors using the EHM method with r_{block}=10% and r_{block} =25% are roughly parallel in log-log plots. For the same level of error corresponding to horizontal lines in Figures 4-6, the r_{block} =10% method yields smaller numerical memory complexities than the method with r_{block} =25%.

3.6. Parameter optimization

346 The choice of the optimal method parameters depends on the targeted accuracy, available
347 computation time and memory and on the fracture network structure. We illustrate the methodology
348 to determine the appropriate parameter values on the most complex fracture network presented
349 before *D1*. Basically, we show in this section that the accuracy is controlled by the discretization
350 ratio r_{block} times the length of the block edge while computation time and memory requirements are
351 controlled by the inverse of the discretization ratio ($1/r_{block}$). The approximation of the method is
352 performed on the block-border discretization by equating the head of points belonging to the same
353 discretization segment. The sole parameter influencing accuracy is thus the normalized segment
354 length d_{block} equal to the discretization ratio r_{block} times the length of the block edge divided by the
355 minimal fracture length. The error *error_flow* defined in (7) increases monotonously with d_{block}
356 (Figure 7). Flow errors smaller than 20% are obtained for d_{block} values smaller than 2. Once the
357 segment length has been fixed by the targeted accuracy, the computation time and memory
358 requirements are adjusted by choosing the discretization of the system in blocks controlled by the
359 parameter $1/r_{\text{block}}$ (Figure 8). Here the computation time refers to the full time of the flow simulation
360 including the determination of the Equivalent Hydraulic Matrices and the solution of the large
361 system issued by the domain-scale flow discretization. Memory requirements are still taken as the
362 number of non-zero elements in the domain-scale matrix (*nnz*). As previously said, *nnz* decreases for
363 coarser domain discretizations. The computation is mainly controlled by the determination of the
364 Equivalent Hydraulic Matrices. It first sharply decreases with $1/r_{\text{block}}$ and then increases slightly. The
365 minimum expresses an optimal distribution of computations between the domain scale and the block
366 scale. Smaller $1/r_{\text{block}}$ values yield more numerous smaller blocks and more Equivalent Hydraulic
367 Matrices to determine and in turn an increase of the full computation time by more than order of
368 magnitude. Large $1/r_{\text{block}}$ values yield less numerous larger blocks which Equivalent Hydraulic
369 Matrices take a much larger time to determine, increasing the full computation time by at least 50%.

Similar results showing the existence of the minimum have been obtained for greater number of Monte-Carlo simulations and for different fracture network structures.

4. Discussion

The principle of the Equivalent Hydraulic Matrices method is to distribute the numerical complexity among two scales, the block-scale and the domain-scale. This method introduces a reduction of the domain-scale numerical memory complexity by coarsening the block-border discretization. The approximation consists in equating heads on nearby network points. It remains local and adjusts automatically to the specific network configuration. Like the tensor and geometrical mapping methods, the EHM method increases connectivity along block interfaces but only through the introduction of shortcuts between existing paths and not through the connection of otherwise disconnected faces. Moreover, the connectivity increase is limited to the block borders and does not affect the connectivity within the block.

The EHM method is structured around the block-scale Equivalent Hydraulic Matrices, which transfer the local connectivity information from the block scale to the domain scale. The Equivalent Hydraulic Matrices are determined by the configurations of the fracture network within the blocks but do not depend on the boundary conditions. In other words, the matrices are not intrinsic medium properties like a tensor but can be used instead of the discrete fracture network in all flow contexts both above and below the Representative Elementary Volume (REV). The Equivalent Hydraulic Matrices method is still applicable below the REV due to the adjustment of the block-scale matrices to the specificity of the connectivity structures.

Because the Equivalent Hydraulic Matrices are derived from DFN computations, it is not surprising that they contain more information than the geometrical projection methods and lead to better performance at equivalent domain-scale numerical memory complexity. We express the domain-

393 scale numerical memory complexity by the number of non-zero elements (*nnz*) of the linear system
394 issued from the discretization of the flow equation. *nnz* is two to four orders magnitude smaller with
395 the EHM method than with geometrical projection methods. The EHM method also displays
396 systematically decreasing flow errors with the domain discretization and block-scale discretization
397 parameter r_{block}. This offers possibilities to find the best optimal complexity for a given error
398 requirement. As seen in section 3.3, this is not possible with the tensor method TENSOR_SIM and it
399 requires too fine a domain discretization with the geometrical method ANIS_GEO.

400 The EHM method is intermediary between the full DFN flow simulation and the tensor method. Like
401 in the classical tensor methods [*Jackson et al.*, 2002], the method relies on block-scale DFN
402 simulations. It is also similar to classical numerical methods from several respects. First, it expresses
403 the relationship between flows and heads on the block borders like many numerical methods such as
404 finite element or boundary element methods. Second, it converges to the full DFN solution when the
405 domain discretization or the block-scale discretization increases. As a two-scale method, it shares
406 similarities with multiscale methods like multigrid methods. It is, however, a pure bottom-up
407 approach in the sense that the block-scale information is used at domain scale but not the other way
408 around. From this respect, it is closer to the principle of the multiscale finite element methods
409 [*Efendiev and Hou*, 2007] than to the principle of multigrid methods [*Wesseling*, 2004]. Finally, it
410 remains opposed to homogenization methods since the Equivalent Hydraulic Matrices strongly
411 depend on the block-scale fracture network structure and cannot be extrapolated to other blocks or
412 other scales.

413 However, EHM methods have two drawbacks, the first one being the specificity of the domain-scale
414 simulation method that precludes the use of commonly available continuous flow simulation
415 softwares like MODFLOW. The second drawback is the additional numerical time complexity
416 arising from the computation of the block-scale equivalent matrices. The total numerical complexity

includes the solution of the domain-scale linear system and the computation of the Equivalent Hydraulic Matrices at the block scale. The first contribution is evaluated by the number of non-zero elements in the domain-scale linear system *nnz* used in the previous section. The second contribution is a function of the number of block-scale simulations multiplied by the complexity of the block-scale simulations. We have chosen to retain only the first contribution to the numerical complexity for the two following reasons. First, the complexity of the domain-scale linear system is a critical constraint. Very large systems corresponding to $nnz>10^7$ require parallel computation. While this constraint is met only for very large systems in 2D, it is current for 3D fracture networks at much smaller domain scales. Second, the EHM methods will likely be interesting for transient simulations. In fact, the computation of the EHMs will be performed only once and the complexity of the transient simulations will depend only on the domain-scale linear system complexity. The choice of both the domain discretization and the block-scale discretization parameter will be dictated by the numerical optimization, the performance of simulations through block-scale and domain-scale computations restricted to manageable sizes, and last but not least by the required accuracy.

5. Conclusion

We have presented a new mapping method for solving the flow equation in 2D discrete fracture networks. The method consists in superposing a mesh onto the fracture network and finding the relationship between heads and flows on the borders of each block of the mesh. The relationship is linear and can be expressed in matrix form, hence the name the "Equivalent Hydraulic Matrices" (EHM) method. We have shown that this linear relationship is fundamentally analog to Darcy's law as it is equivalent to relating flows to well-chosen head gradients on block borders. The matrix coefficients can be determined by block-scale numerical simulations and express equivalent block-scale permeability between block border zones. The zones are chosen independently for each block interface and correspond to the discretization of intersection points between the fracture network and

441 the block border. The method is parameterized both by the block-scale discretization parameter
442 (block-scale discretization distance divided by the characteristic block scale) and the domain
443 discretization (the domain scale divided by characteristic block scale in each direction). The flow
444 simulation at the domain scale is performed simply by assembling the block-scale Equivalent
445 Hydraulic Matrices through head and flow continuity conditions.

446 The interest of the EHM method is to keep good approximations of both the internal block and inter-
447 block connectivities. Discretization is performed at a local scale and adjusts automatically to local
448 fracture network configurations. We show on a broad range of 2D fracture networks with different
449 density, fracture length and transmissivity distributions that the relative error of the method decreases
450 systematically with the domain discretization and the block-scale discretization parameter, allowing
451 for a possible automatic control of the method accuracy. We also show that the relative error of the
452 EHM method remains restricted to a few percents for a coarse domain discretization (30×30 to
453 50×50), whatever the network geometrical structure and the fracture transmissivity distribution. The
454 main advantage is its applicability to all kind of network structures, whereas the tensor method can
455 only be used for blocks larger than the Representative Elementary Volume, a too restrictive
456 condition for general DFN simulations. Geometrical methods give results of comparable accuracy
457 for a much larger domain discretization leading to domain-scale numerical memory complexities
458 orders of magnitude larger than the numerical memory complexity of the EHM method. The EHM
459 method enables large-scale 2D flow simulation networks. We intend to test its performance on 3D
460 fracture network simulations and in transient flow contexts.

461 **Appendices**

462 ***Appendix A: Property of the Equivalent Hydraulic Matrix***

463 With the construction method described in section 2.2, $\boldsymbol{A_k}$ has several properties. First, by imposing
464 a fixed head of 1 at pole j and 0 at the other ones as boundary conditions, the flow goes into the
465 block by $\boldsymbol{p_k}(j)$ and outward through the other poles $\boldsymbol{p_k}(i)$ $(i \neq j)$. Considering the flow going into
466 the block as positive and the flow going outward as negative leads to:

467 $$\begin{cases} \boldsymbol{A_k}(j,j) \geq 0 \\ \boldsymbol{A_k}(i,j) \leq 0, \ i \neq j \end{cases} \quad (8)$$

468 Second, for a given column j, all elements $\boldsymbol{A_k}(i,j)$ are determined simultaneously by solving the
469 flow equation; mass conservation implies that

470 $$\sum_{i=1}^{N_P^k} \boldsymbol{A_k}(i,j) = 0. \quad (9)$$

471 Or similarly:

472 $$\boldsymbol{A_k}(i,i) = -\sum_{j=1, j\neq i}^{N_P^k} \boldsymbol{A_k}(j,i). \quad (10)$$

473 Third, because the reciprocity principle is applicable in the case of Darcian flow [*Barker*, 1991], $\boldsymbol{A_k}$
474 is symmetric:

475 $$\boldsymbol{A_k}(i,j) = \boldsymbol{A_k}(j,i). \quad (11)$$

476 Fourth, we show that the linear relationship (1) between flows and heads with property (10) leads to
477 a relationship between flows and head gradients. In fact:

$$\boldsymbol{\phi_k}(i) = \sum_{j=1}^{N_P^k} \boldsymbol{A_k}(i,j) \times \boldsymbol{H_k}(j)$$

$$\boldsymbol{\phi_k}(i) = \sum_{j=1, j\neq i}^{N_P^k} \boldsymbol{A_k}(i,j) \times \boldsymbol{H_k}(j) + \boldsymbol{A_k}(i,i) \times \boldsymbol{H_k}(i)$$

478 and using (10):

$$\boldsymbol{\phi_k}(i) = \sum_{j=1, j\neq i}^{N_P^k} \boldsymbol{A_k}(i,j) \times (\boldsymbol{H_k}(j) - \boldsymbol{H_k}(i))$$

479 $$\boldsymbol{\phi_k}(i) = \sum_{j=1}^{N_P^k} \boldsymbol{A_k}(i,j) \times x_{k,ij} \times \frac{(\boldsymbol{H_k}(j) - \boldsymbol{H_k}(i))}{x_{k,ij}} \quad (12)$$

480 where $x_{k,ij}$ is the distance between poles $\boldsymbol{p_k}(i)$ and $\boldsymbol{p_k}(j)$. Equation (12) shows that flow $\boldsymbol{\phi_k}(i)$ at
481 $\boldsymbol{p_k}(i)$ is the sum of the head gradients from $\boldsymbol{p_k}(i)$ to the other poles. Equation (12) gives a simple
482 interpretation of $\boldsymbol{A_k}(i,j) \times x_{k,ij}$. $\boldsymbol{A_k}(i,j) \times x_{k,ij}$ is the proportionality coefficient between flow
483 $\boldsymbol{\phi_k}(i)$ and the head gradient $(\boldsymbol{H_k}(j) - \boldsymbol{H_k}(i))/x_{k,ij}$ between $\boldsymbol{p_k}(i)$ and $\boldsymbol{p_k}(j)$. $\boldsymbol{A_k}(i,j) \times x_{k,ij}$ can
484 thus be interpreted as an "equivalent transmissivity" between the i^{th} and j^{th} poles.

485

Appendix B: Tensor permeability and finite elements (TENSOR_SIM method)

The Equivalent Hydraulic Matrices method consists in dividing the domain into blocks and describing block-scale hydraulic properties using Equivalent Hydraulic Matrices. The discretization of the block borders by poles $\boldsymbol{p_k}$ is determined by the block-scale discretization parameter r_{block}, which is the ratio of the block-scale distance discretization to the block length. This parameter r_{block} drives the discretization of intersections $\boldsymbol{m_k}$ between block borders and fractures. Coefficients of the EHMs are determined by simulations at the block scale as described in section 2.2. The EHMs are equivalent to tensors in that they impose the following discretization and construction rules: (1) $r_{block}=100\%$, i.e. each block border is discretized by at most one pole, (2) each block border is represented by one pole (even if there is no intersection point), (3) matrix coefficients are determined by applying head gradient boundary conditions in the vertical and horizontal directions [*Renard et al.*, 2001], (4) the computed flow rates used for the determination of the coefficients are the directional flow rates, i.e. the mean of the flow rates going out of the domain through borders perpendicular to the studied direction, and (5) coefficients are corrected to obtain symmetric positive definite tensors [*Long et al.*, 1982]. Adding these rules of determination, the Equivalent Hydraulic Matrices become tensors that describe block-scale permeability. Computed block-scale tensors are used within a classical mixed hybrid method adapted for quadrangles to simulate flow at the domain scale [*Chavent and Roberts*, 1991]. We denote this method the TENSOR_SIM method.

Notations

K_{xx}	permeability in the *x*-direction due to a head gradient in the *x*-direction, m/s.
K_{yy}	permeability in the *y*-direction due to a head gradient in the *y*-direction, m/s.
K_{xy}	permeability in the *x*-direction due to a head gradient in the *y*-direction, m/s.
K_{yx}	permeability in the *y*-direction due to a head gradient in the *x*-direction, m/s.
$\boldsymbol{p_k}$	vector of poles.
$\boldsymbol{\Phi_k}$	vector of flow rates at the poles for block *k*, m^2/s.
$\boldsymbol{H_k}$	vector of heads at the poles for block *k*, m.
$\boldsymbol{A_k}$	Equivalent Hydraulic Matrix of block *k*, m/s.
$\boldsymbol{m_k}$	vector of intersections between the fractures and the faces of block *k*.
d_{block}	discretization distance of block borders, m.
r_{block}	discretization ratio of block borders.
N_P^k	number of poles of block *k*.
$x_{k,ij}$	distance between the i^{th} and j^{th} poles, m.
P	union of all poles.

520	P^i	union of poles on block interfaces.
521	P^f	union of poles on domain faces.
522	N	total number of poles.
523	N^{i}	number of poles of type P^{i}.
524	N^{f}	number of poles of type P^{f}.
525	$B(j)$	set of blocks sharing pole $P^i(j)$
526	$q_{b,P^i(j)}$	flow rate at poles $P^i(j)$ from the b^{th} block, m^2/s.
527	N^{fd}	number of poles on the Dirichlet boundary condition.
528	N^{fn}	number of poles on the Neumann boundary condition.
529	H^{fd}	head of poles on the Neumann boundary condition, m
530	$(H^{fd})_0$	fixed head on the Neumann boundary condition, m
531	p	percolation parameter.
532	l	fracture length, m.
533	$p(l)$	fracture length distribution.
534	a	power law exponent.

535 $\Phi_m^{f_i}$ flow rate computed by the method "*m*" on the face f_i, m^2/s.

536 $\Phi_{ref}^{f_i}$ flow rate computed by the reference method on the face f_i, m^2/s.

537 *nnz* number of non-zero elements of the domain-scale linear system.

538 p_{border} border discretization percentage

Acknowledgments

This work was supported by the ANR project MICAS. We thank Jocelyne Erhel for fruitful discussions.

542 **Bibliography**

543 Ando, K., et al. (2003), Stochastic continuum modeling of flow and transport in a crystalline rock
544 mass: Fanay-Augères, France, revisited, *Hydrogeology Journal*, *11*(5).

545 Baghbanan, A., and L. R. Jing (2007), Hydraulic properties of fractured rock masses with correlated
546 fracture length and aperture, *International Journal of Rock Mechanics and Mining Sciences*, *44*(5),
547 704-719.

548 Barker, J. A. (1991), The reciprocity principle and an analytical solution for darcian flow in a
549 network, *Water Resour. Res.*, *27*(5), 743-746.

550 Berkowitz, B., et al. (2000), Scaling of fracture connectivity in geological formations, *Geophys. Res.*
551 *Lett.*, *27*(14), 2061-2064.

552 Bonnet, E., et al. (2001), Scaling of Fracture Systems in Geological Media, *Reviews of Geophysics*,
553 *39*(3), 347-383.

554 Botros, F. E., et al. (2008), On mapping fracture networks onto continuum, *Water Resour. Res.*,
555 *44*(8).

556 Bour, O., and P. Davy (1997), Connectivity of random fault networks following a power law fault
557 length distribution, *Water Resources Research*, *33*(7), 1567-1583.

558 Bour, O., and P. Davy (1998), On the connectivity of three dimensional fault networks, *Water*
559 *Resources Research*, *34*(10), 2611-2622.

560 Bourbiaux, B., et al. (1998), A rapid and efficient methodology to convert fractured reservoir images
561 into a dual-porosity model, *Rev. Inst. Fr. Pet.*, *53*(6), 785-799.

562 Chavent, G., and J. E. Roberts (1991), A unified physical presentation of mixed, mixed-hybrid finite-
563 elements and standard finite-difference approximations for the determination of velocities in
564 waterflow problems, *Advances in Water Resources*, *14*(6), 329-348.

565 Cvetkovic, V., et al. (2004), Stochastic simulation of radionuclide migration in discretely fractured
566 rock near the Äspö Hard Rock Laboratory, *Water Resources Research*.

567 Davis, T. A. (2004), Algorithm 832: UMFPACK V4.3---an unsymmetric-pattern multifrontal
568 method, *ACM Trans. Math. Softw.*, *30*(2), 196-199.

569 Davy, P., et al. (2006), Flow in multiscale fractal fracture networks, *Fractal Analysis for Natural*
570 *Hazards*(261), 31-45.

571 Davy, P., et al. (2009), A Universal Model of Fracture Scaling and its consequence for crustal hydro-
572 mechanics, *Journal of Geophysical Research, submitted*.

de Dreuzy, J. R., et al. (2001a), Hydraulic properties of two-dimensional random fracture networks following a power law length distribution: 2-Permeability of networks based on log-normal distribution of apertures, *Water Resources Research*, *37*(8), 2079-2095.

de Dreuzy, J. R., et al. (2001b), Hydraulic properties of two-dimensional random fracture networks following a power law length distribution 1. Effective connectivity, *Water Resour. Res.*, *37*(8), 2065-2078.

de Dreuzy, J. R., et al. (2002), Permeability of 2D fracture networks with power-law distributions of length and aperture, *Water Resources Research*, *38*(12).

de Dreuzy, J. R., and J. Erhel (2002), Efficient algorithms for the determination of the connected fracture network and the solution of the steady-state flow equation in fracture networks, *Computers and Geosciences*, *29*(107-111).

Dershowitz, W. S., and C. Fidelibus (1999), Derivation of equivalent pipe network analogues for three-dimensional discrete fracture networks by the boundary element method, *Water Resour. Res.*, *35*(9), 2685-2691.

Durlofsky, L. J. (1991), Numerical calculation of equivalent grid block permeability tensors for heterogeneous porous media, *Water Resour. Res.*, *27*(5), 699-708.

Efendiev, Y., and T. Hou (2007), Multiscale finite element methods for porous media flows and their applications, *Applied Numerical Mathematics*, *57*(5-7), 577-596.

Erhel, J., et al. (2009), A parallel scientific software for heterogeneous hydrogeoloy, in *Parallel Computational Fluid Dynamics 2007*, edited, pp. 39-48.

Falgout, R. D., et al. (2005), Pursuing scalability for Hypre's conceptual interfaces, *ACM Trans. Math. Softw.*, *31*(3), 326-350.

Hsieh, P. A. (1998), Scale effects in fluid flow through fractured geological media, in *Scale dependence and scale invariance in hydrology*, edited, pp. 335-353, Cambridge University Press.

Jackson, C. P., et al. (2002), Self-consistency of a heterogeneous continuum porous medium representation of a fractured medium, *Water Resour. Res.*, *36*.

Karimi-Fard, M., et al. (2006), Generation of coarse-scale continuum flow models from detailed fracture characterizations, *Water Resources Research*, *42*(10).

Lee, S. H., et al. (2001), Hierarchical modeling of flow in naturally fractured formations with multiple length scales, *Water Resources Research*, *37*(3), 443-455.

Li, J. H., et al. (2009), Permeability tensor and representative elementary volume of saturated cracked soil, *Can. Geotech. J.*, *46*(8), 928-942.

605 Long, J. C. S., et al. (1982), Porous media equivalents for networks of discontinuous fractures, *Water*
606 *Resour. Res.*, *18*(3), 645-658.

607 Neuman, S. P. (2005), Trends, prospects and challenges in quantifying flow and transport through
608 fractured rocks, *Hydrogeology Journal*, *13*(1), 124-147.

609 Reeves, D. M., et al. (2008), Transport of conservative solutes in simulated fracture networks: 1.
610 Synthetic data generation, *Water Resour. Res.*, *44*(5).

611 Renard, P., et al. (2001), Laboratory determination of the full permeability tensor, *Journal of*
612 *Geophysical Research*, *106*(B11), 26443-26452.

613 Svensson, U. (2001), A continuum representation of fracture networks. Part I: Method and basic test
614 cases, *Journal of Hydrology*, *250*(1-4), 170-186.

615 Tsang, Y. W., et al. (1996), Tracer transport in a stochastic continuum model of fractured media,
616 *Water Resources Research*, *32*(10), 3077-3092.

617 Wesseling, P. (2004), *An Introduction to Multigrid Methods*, Edwards.

618

619

620

621

622 **Figure captions**

623 Figure 1 – Fracture network at the block scale (a) and corresponding flows (b) for the gradient head
624 boundary conditions illustrated in (a). Fracture network parameters are the system size L normalized
625 by the smallest fracture length (L =100), the fracture density number twice larger as its value at
626 percolation threshold, the power-law fracture length exponent of 2.5 and the lognormal
627 transmissivity distribution of logarithmic standard deviation 3.0. Boundary flows integrated on the
628 domain sides and normalized by the mean fracture transmissivity are given in (b). They display large
629 differences between opposite sides and illustrate the non-tensor nature of the flows.

630 Figure 2 – Principle of the block-border discretization with two different discretization scales d_{block}
631 corresponding to the side length (a) and to half of it (b). The backbone of the sub-network contained
632 in the block is represented by the grey segments. Intersections $\boldsymbol{m}_{\text{k}}$ between the backbone and the
633 block borders are the black dots. Discretization segments and poles $\boldsymbol{p_k}$ are respectively the color
634 dashed segments and crosses. In (a), the four discretization segments intersect the backbone in one or
635 two points. The four poles corresponding to the four crosses are thus defined and the Equivalent
636 Hydraulic Matrix (EHM) is of rank 4. In (b), only six of the eight discretization segments intersect
637 the backbone leading to the definition of 6 poles and to an EHM of rank 6.

638 Figure 3 – Principle of the determination of one of the columns of the Equivalent Hydraulic Matrix
639 $\boldsymbol{A_k}$. In this example, block k is made up of fives intersections between the sub-network and the block
640 borders (black points) and four poles (blue crosses). The boundary conditions applied to poles
641 illustrated in (a) are a fixed head of 1 for the 2$^{\text{nd}}$ pole and 0 for the other ones. They condition the
642 boundary conditions applied to the intersections illustrated in (b), which are a fixed head of 1 for the

643 intersections represented by the 2nd pole and 0 for the other ones. Flow rates in poles (d) are deduced
644 from flow rates at the intersections (c). The flow rate at the i^{th} pole is the sum of the flow rates at the
645 intersections represented by this pole. The elements of the second column of the matrix $\boldsymbol{A_k}$ are
646 deduced from flow rates computed at the poles (e).

647 Figure 4 – *flow_error* versus numerical memory complexity (*nnz*) for lattice structures and dense
648 fracture networks with constant fracture transmissivity (magenta symbols). The grey area underlines
649 a lower part of the graph where errors range between 5×10^{-6}% and 10^{-4}%. The dashed horizontal line
650 pictures the 10% error value. The dashed diagonal lines are power-law functions of exponent -1 and
651 are meant as a guide for the eye for the decrease tendency of the EHM method. Note that errors
652 larger than 10^3 are not represented.

653 Figure 5 – *flow_error* versus numerical memory complexity (*nnz*) for stochastic complex fracture
654 networks at threshold with distributed fracture transmissivities. The dashed horizontal line pictures
655 the 10% error value. The dashed diagonal lines are power-law functions of exponent -1 and are
656 meant as a guide for the eye for the decrease tendency of the EHM method. Note that errors larger
657 than 10^3 are not represented.

658 Figure 6 – *flow_error* versus numerical memory complexity (*nnz*) for stochastic complex fracture
659 networks with distributed fracture transmissivities. The dashed horizontal line pictures the 10% error
660 value. The dashed diagonal lines are power-law functions of exponent -1 and are meant as a guide
661 for the eye for the decrease tendency of the EHM method. Note that errors larger than 10^3 are not
662 represented.

663 Figure 7 –*flow_error* versus d_{block} the discretization ratio r_{block} times the length of the block edge for
664 the network *D1* (domain size L=100).

Figure 8 – Computation time (red dashed line) and numerical memory complexity taken as the number of non-zero elements in the largest matrix (black line) as a function of block size divided by the segment discretization length $1/r_{block}$ for *D1* with d_{block} equal to 1.

669 **Tables**

Network type	Parameters				Table 2
	p	a	θ	σ_{lnT}	
A0	192	1	0°, 30°	0	
A1	192	1	0°, 30°	3	
A2	12	1	0°, 30°	0	
A3	12	1	0°, 30°	3	I1
B0	6	2.5	Uniform	3	
B1	6	3	Uniform	3	I2
B2	6	3.5	Uniform	3	
C0	10	2.5	Uniform	3	
C1	10	3	Uniform	3	
C2	10	3.5	Uniform	3	I3
D0	20	2.5	Uniform	0	
D1	20	2.5	Uniform	3	I4

670 Table 1 – Characteristics of the tested fracture networks. The first four networks are on-lattice structures whereas the other ones are off-lattice
671 structures. The ratio of the domain size L to the length of the smallest fracture l_{min} is set to 100. The fracture density is characterized by the
672 percolation parameter p [*Bour and Davy*, 1998]. Fractures either cross the whole domain (a=1) or are distributed according to a power-law
673 distribution (a>1). Fracture orientations (θ) are either specified to a set of fixed angles (first four cases) or uniformly distributed. Fracture
674 transmissivity is constant ($\sigma_{lnT} = 0$) or lognormally distributed with a lognormal standard deviation ($\sigma_{lnT} = 3$). The last column indicates the
675 figure numbers displaying an example of the network type in Table 2. Fracture network types are classified in family of networks: "*A*" is for
676 lattice structures, "*B*" for networks at percolation threshold, "*C*" for networks with an intermediary fracture density and "*D*" for dense networks.
677

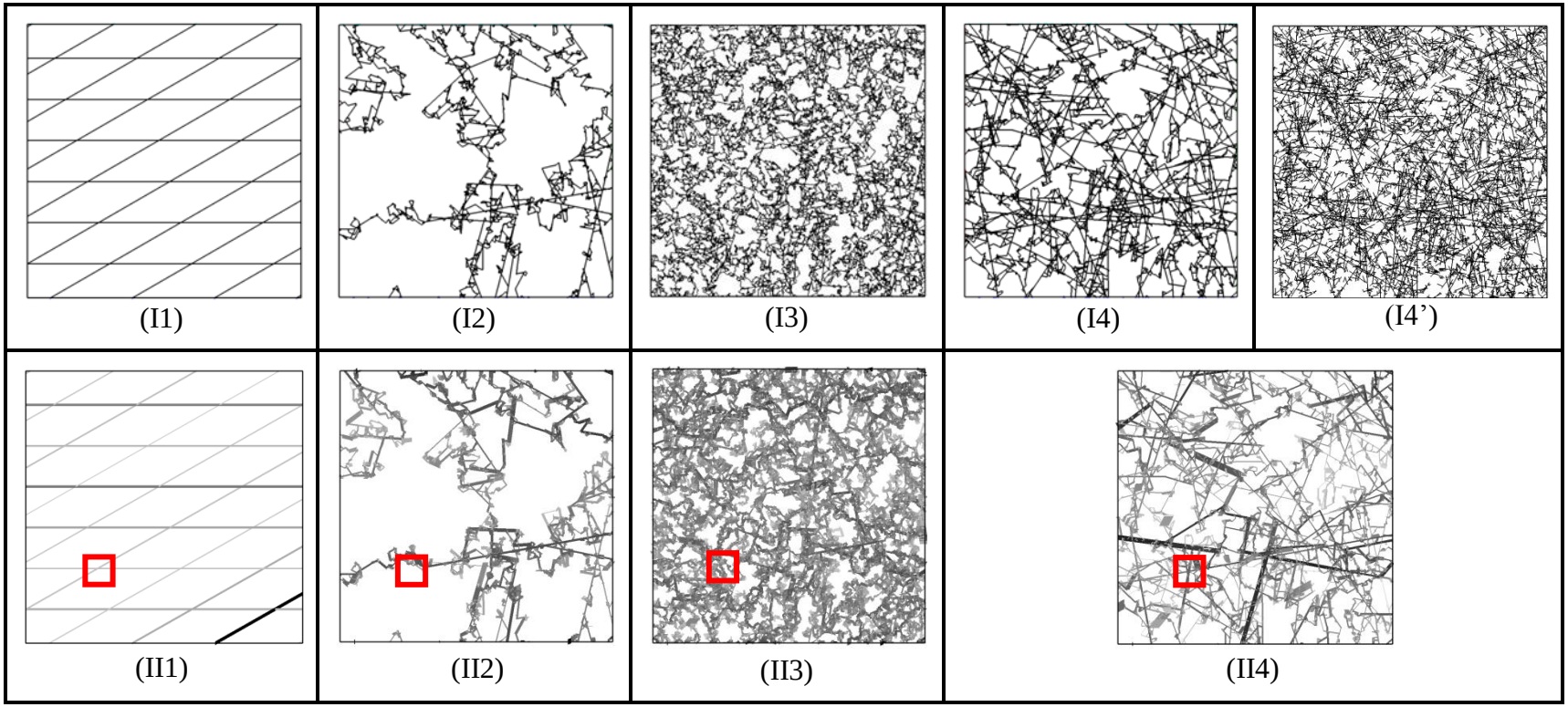

678 Table 2 – Illustration of the tested fracture networks with examples of backbones (I1-I4), infinite clusters (I4') and flows (II1-II4) obtained with
679 the gradient boundary conditions illustrated by Figure 1a and computed with a broadly distributed fracture transmissivity $\sigma_{lnT} = 3$ (see Table 1).
680 Flow magnitude is represented by grey intensity and segment width. I1, I2, I3 and I4-4' correspond to network types *A3*, *B1*, *C2* and *D1* (Table
681 1). Red squares stand for an elementary block corresponding to a domain discretization of 10×10 blocks.

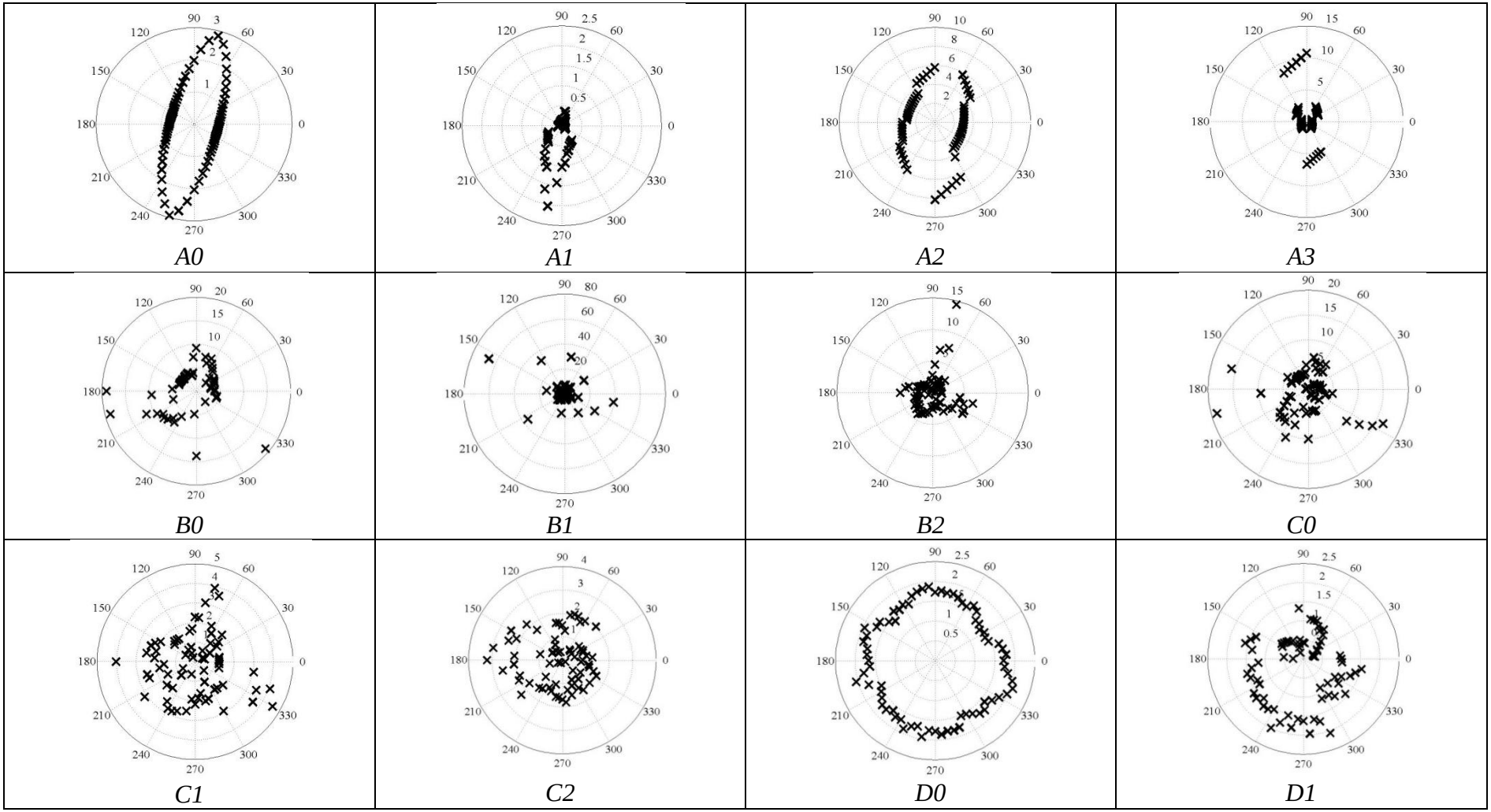

682 Table 3 – Polar plots of permeability for the networks of Table 1, representing the permeability versus the polar angle θ. Each point represents
683 for a given θ the permeability computed in a square of side length $L/3$ (where L is the domain size), of axis rotated by θ and centered on the
684 initial system center.

	ANIS_GEO				TENSOR_SIM			EHM (10%)			EHM (25%)		
Domain discretization	**10×10**	**30×30**	**50×50**	**200×200**	**10×10**	**30×30**	**50×50**	**10×10**	**30×30**	**50×50**	**10×10**	**30×30**	**50×50**
A0	33	33	31	20	0.14	0.04	0.92	5.5×10^{-5}	2.0×10^{-5}	2.7×10^{-5}	33	2.3×10^{-5}	2.8×10^{-5}
A1	44	49	47	2.3				4.9×10^{-5}	1.5×10^{-5}	3.2×10^{-5}	25	1.6×10^{-5}	3.3×10^{-5}
A2	49	2.3	2.0	0.3	7.5	35	37	3.4×10^{-5}	3.1×10^{-5}	1.4×10^{-5}	3.4×10^{-5}	3.2×10^{-5}	1.4×10^{-5}
A3	23	6.0	5.6	1.2				2.1×10^{-4}	6.3×10^{-5}	4.4×10^{-5}	2.1×10^{-4}	6.3×10^{-5}	4.4×10^{-5}
B0			22	4.7				0.42	0.25	0.11	3.1	1.2	0.59
B1			1.2×10^{3}	41				3.6	0.73	0.29	10	4.2	2.6
B2			3.4×10^{4}	2.2×10^{2}				45	1.6	1.5	81	45	4.8
C0			78	49				1.0	0.5	0.2	6.1	1.3	0.87
C1			2.1×10^{3}	93				5.9	1.3	1.5	33	5.7	5.1
C2			1.2×10^{4}	4.4×10^{2}				23	4.5	2.1	1.8×10^{2}	29	13
D0			1.7×10^{2}	28	11	21	50	2.8	0.89	0.51	21	5.1	2.9
D1			4×10^{2}	19				3.8	0.75	0.45	23	5.7	2.8

Table 4 – *flow_error* as defined by equation (7) for the backbone of the fracture network types defined in Table 1 and for the three computational methods ANIS_GEO, TENSOR_SIM and EHM at different discretization levels. Domain discretization refers to the ratio of the domain size to the block size in each direction. EHM methods are characterized in brackets by their block-scale discretization parameter r_{block} equal to the ratio expressed in % between the block-scale discretization distance d_{block} and the block scale. Empty cells mean that the conditions of application of the method are not fulfilled in the corresponding case.

	DFN	ANIS_GEO				TENSOR_SIM			EHM (10%)			EHM (25%)		
Domain discretization		**10×10**	**30×30**	**50×50**	**200×200**	**10×10**	**30×30**	**50×50**	**10×10**	**30×30**	**50×50**	**10×10**	**30×30**	**50×50**
A0	26	0.46	4.4	12	200	1.2	12	34	14	110	140	1.2	42	75
A1	26	0.46	4.4	12	200				15	101	140	1.2	41	87
A2	0.16	0.46	4.4	12	200	1.2	12	34	0.7	1.6	2.4	0.6	1.5	2.4
A3	0.16	0.46	4.4	12	200				0.7	1.6	2.4	0.6	1.5	2.4
B0	0.87			12	200				0.45	1.4	2.5	0.3	1.2	2.2
B1	13			12	200				1.1	4.2	6.7	0.6	2.6	4.5
B2	33			12	200				1.5	6.6	12	0.7	3.5	7.1
C0	6.1			12	200				1.6	4.0	6.0	0.9	3.0	5.0
C1	53			12	200				4.5	16	26	1.8	8.6	16
C2	240			12	200				11	56	96	2.8	22	46
D0	52			12	200	1.2	12	34	8.7	27	41	2.9	15	26
D1	51			12	200				8.7	27	41	2.9	15	26

692 Table 5 – Numerical memory complexity expressed as the number of non-zero elements (*nnz*) of the domain-scale linear systems issued from the
693 flow discretization for the network cases of Table 1. Parameters are identical to those of Table 4. All numbers are expressed in thousands of non-
694 zero elements.

695

	EHM (10%)			EHM (25%)		
Domain discretization	**10×10**	**30×30**	**50×50**	**10×10**	**30×30**	**50×50**
A0	70	21	14	91	53	36
A1	69	23	14	91	53	32
A2	4.7	1.7	2.6	13	4.3	2.6
A3	4.7	1.7	2.6	13	4.3	2.6
B0	14	7	5.3	26	14	10
B1	44	23	15	59	37	28
B2	54	32	23	70	49	39
C0	25	12	8.3	41	22	15
C1	53	29	21	70	46	35
C2	72	44	33	86	65	53
D0	50	26	18	70	44	32
D1	50	26	18	70	44	32

696

697 Table 6 – Block-scale border merging percentage p_{border} for the fracture network types of Table 1.

	ANIS_GEO				TENSOR_SIM			EHM (10%)			EHM (25%)			Table 2
Domain discretization	**10×10**	**30×30**	**50×50**	**200×200**	**10×10**	**30×30**	**50×50**	**10×10**	**30×30**	**50×50**	**10×10**	**30×30**	**50×50**	
D0			5.5×10^{2}	1.5×10^{2}	37	38	14	11	4.9	3.0	76	23	14	
D1			1.7×10^{3}	1.5×10^{2}				12	4.3	2.4	70	20	11	I4’

Table 7 – *flow_error* as defined by equation (7) for the infinite cluster of fracture networks *D0* and *D1* (see Table 1 for description). EHM methods are characterized in brackets by their block-scale discretization parameter r_{block} equal to the ratio expressed in % of the block-scale discretization distance d_{block} to the block scale.

Figures

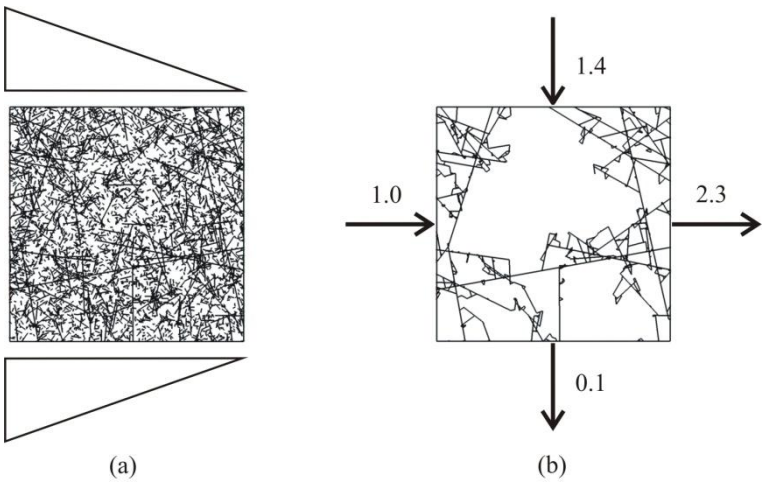

Figure 1 – Fracture network at the block scale (a) and corresponding flows (b) for the gradient head boundary conditions illustrated in (a). Fracture network parameters are the system size L normalized by the smallest fracture length (L =100), the fracture density number twice larger as its value at percolation threshold, the power-law fracture length exponent of 2.5 and the lognormal transmissivity distribution of logarithmic standard deviation 3.0. Boundary flows integrated on the domain sides and normalized by the mean fracture transmissivity are given in (b). They display large differences between opposite sides and illustrate the non-tensor nature of the flows.

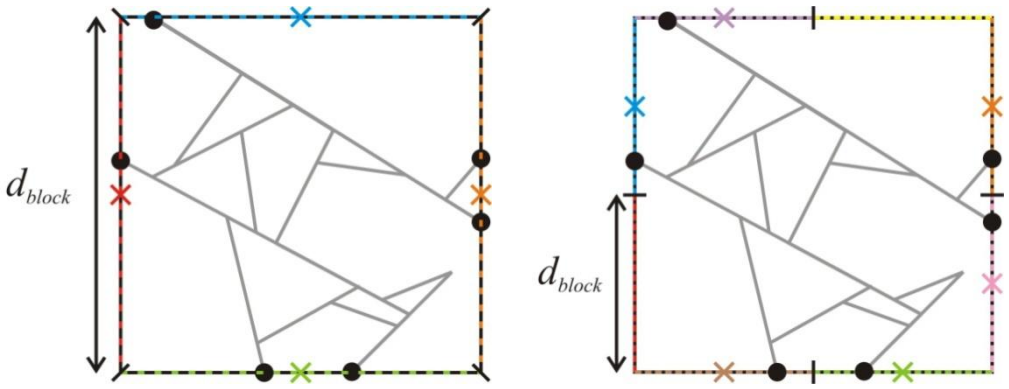

(a) (b)

Figure 2 – Principle of the block-border discretization with two different discretization scales d_{block} corresponding to the side length (a) and to half of it (b). The backbone of the sub-network contained in the block is represented by the grey segments. Intersections $\boldsymbol{m}_{\text{k}}$ between the backbone and the block borders are the black dots. Discretization segments and poles $\boldsymbol{p_k}$ are respectively the color dashed segments and crosses. In (a), the four discretization segments intersect the backbone in one or two points. The four poles corresponding to the four crosses are thus defined and the Equivalent Hydraulic Matrix (EHM) is of rank 4. In (b), only six of the eight discretization segments intersect the backbone leading to the definition of 6 poles and to an EHM of rank 6.

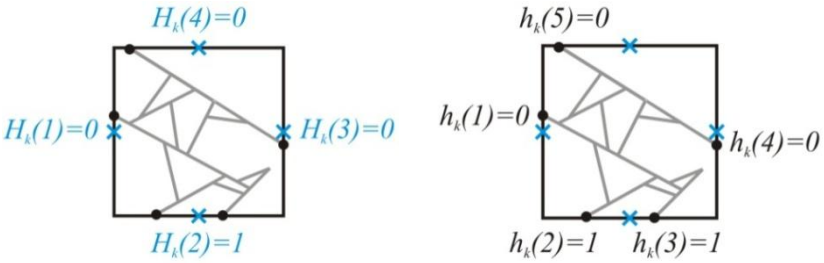

(a)

(b)

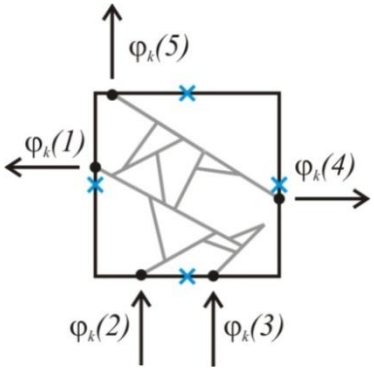

(c)

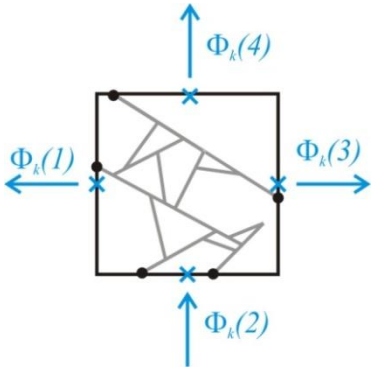

(d)

$$\begin{cases} A_k(2,1) = \phi_k(1) \\ A_k(2,2) = \phi_k(2) \\ A_k(2,3) = \phi_k(3) \\ A_k(2,4) = \phi_k(4) \end{cases}$$

(e)

720 Figure 3 – Principle of the determination of one of the columns of the Equivalent Hydraulic Matrix
721 $\boldsymbol{A_k}$. In this example, block *k* is made up of fives intersections between the sub-network and the block
722 borders (black points) and four poles (blue crosses). The boundary conditions applied to poles
723 illustrated in (a) are a fixed head of 1 for the 2nd pole and 0 for the other ones. They condition the
724 boundary conditions applied to the intersections illustrated in (b), which are a fixed head of 1 for the
725 intersections represented by the 2nd pole and 0 for the other ones. Flow rates in poles (d) are deduced
726 from flow rates at the intersections (c). The flow rate at the i^{th} pole is the sum of the flow rates at the
727 intersections represented by this pole. The elements of the second column of the matrix $\boldsymbol{A_k}$ are
728 deduced from flow rates computed at the poles (e).

729

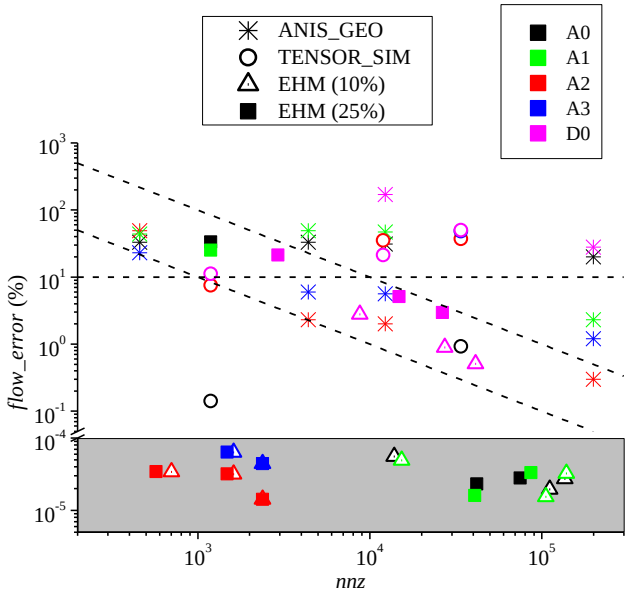

730

731 Figure 4 – *flow_error* versus numerical memory complexity (*nnz*) for lattice structures and dense
732 fracture networks with constant fracture transmissivity (magenta symbols). The grey area underlines
733 a lower part of the graph where errors range between 5×10^{-6}% and 10^{-4}%. The dashed horizontal line
734 pictures the 10% error value. The dashed diagonal lines are power-law functions of exponent -1 and
735 are meant as a guide for the eye for the decrease tendency of the EHM method. Note that errors
736 larger than 10^3 are not represented.

737

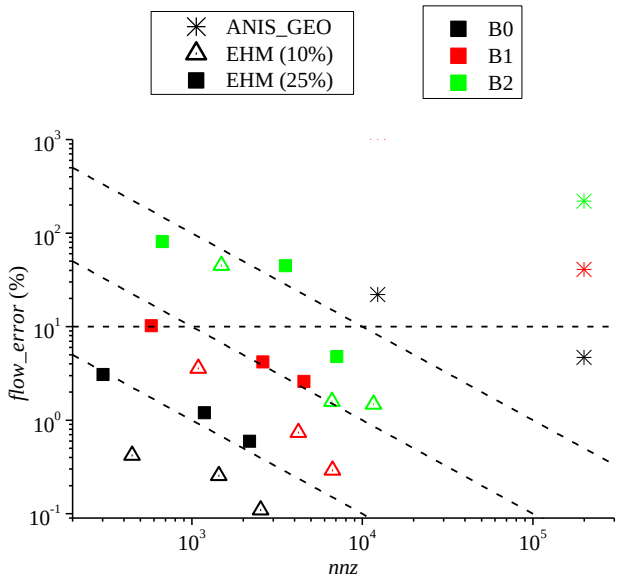

738

739 Figure 5 – *flow_error* versus numerical memory complexity (*nnz*) for stochastic complex fracture
740 networks at threshold with distributed fracture transmissivities. The dashed horizontal line pictures
741 the 10% error value. The dashed diagonal lines are power-law functions of exponent -1 and are
742 meant as a guide for the eye for the decrease tendency of the EHM method. Note that errors larger
743 than 10^3 are not represented.

744

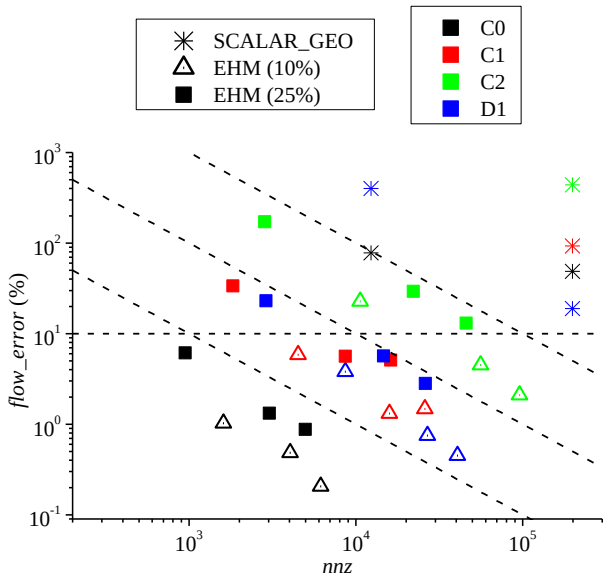

745

746 Figure 6 – *flow_error* versus numerical memory complexity (*nnz*) for stochastic complex fracture
747 networks with distributed fracture transmissivities. The dashed horizontal line pictures the 10% error
748 value. The dashed diagonal lines are power-law functions of exponent -1 and are meant as a guide
749 for the eye for the decrease tendency of the EHM method. Note that errors larger than 10^3 are not
750 represented.

751

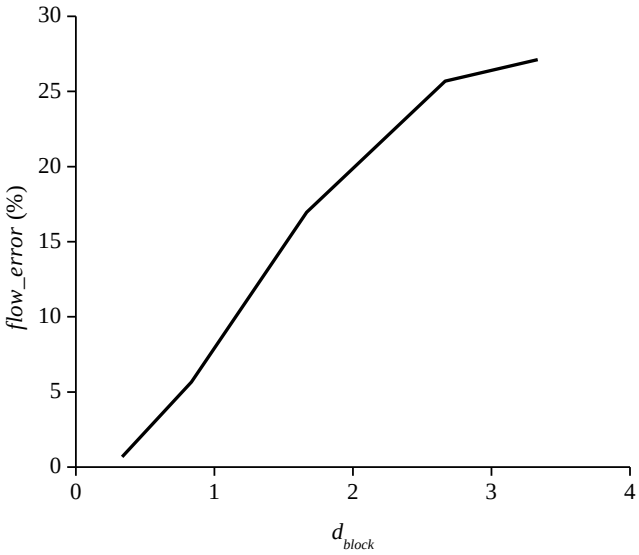

Figure 7 –*flow_error* versus d_{block} the discretization ratio r_{block} times the length of the block edge for the network *D1* (domain size *L*=100).

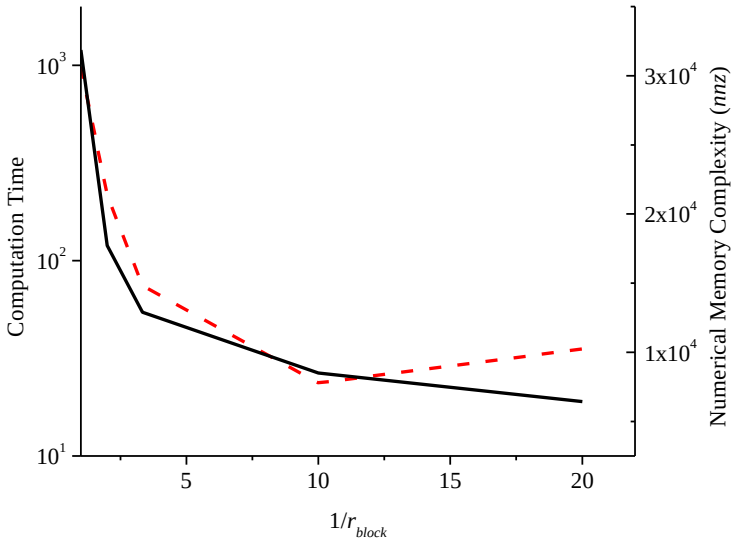

Figure 8 – Computation time (red dashed line) and numerical memory complexity taken as the number of non-zero elements in the largest matrix (black line) as a function of block size divided by the segment discretization length $1/r_{block}$ for *D1* with d_{block} equal to 1.